Convergence of Quantum Dot Barcodes with Microfluidics and Signal Processing for Multiplexed High-Throughput Infectious Disease Diagnostics

Jesse M. Klostranec,[†] Qing Xiang,[†] Gabriella A. Farcas,[‡] Jeongjin A. Lee,[†] Alex Rhee,[†] Erin I. Lafferty,[‡] Steven D. Perrault,[†,‡] Kevin C. Kain,[‡,||] and Warren C. W. Chan*,[†,§]

Institute of Biomaterials and Biomedical Engineering and The Terrence Donnelly Centre for Cellular and Molecular Research, Institute of Medical Sciences and the McLaughlin Centre for Molecular Medicine, Department of Materials Science, University of Toronto, 160 College Street, Toronto, Ontario M5S 3E1, Canada, and McLaughlin-Rotman Centre for Global Health, Tropical Disease Unit, UHN–Toronto General Hospital, 190 Elizabeth Street, Toronto, Ontario M5M 1M1, Canada

ABSTRACT

Through the convergence of nano- and microtechnologies (quantum dots and microfluidics), we have created a diagnostic system capable of multiplexed, high-throughput analysis of infectious agents in human serum samples. We demonstrate, as a proof-of-concept, the ability to detect serum biomarkers of the most globally prevalent blood-borne infectious diseases (i.e., hepatitis B, hepatitis C, and HIV) with low sample volume (<100 μL), rapidity (<1 h), and 50 times greater sensitivity than that of currently available FDA-approved methods. We further show precision for detecting multiple biomarkers simultaneously in serum with minimal cross-reactivity. This device could be further developed into a portable handheld point-of-care diagnostic system, which would represent a major advance in detecting, monitoring, treating, and preventing infectious disease spread in the developed and developing worlds.

The past decade has witnessed a dramatic emergence of many technologies that utilize phenomena unique to material structures at the micro and nano length scales.[1–4] However, converging these technologies into a useful biomedical device that combines all of the special properties of each technology poses a major challenge. A convergence could lead to a universal handheld point-of-care device (an instrument that can diagnose disease at the bedside) capable of identifying disease biomarkers in a variety of clinical samples, including blood, urine, or sputum.[5] This would represent a major advance in medical diagnosis and treatment. In this work, we demonstrate the assembly of a high-throughput, high-sensitivity platform capable of detecting multiple biomarkers

(multiplexed detection) of infectious disease (ID) agents by integrating recent advances in quantum dot (Qdot)-barcode (QdotB),[6,7] microfluidic,[8–10] and photon detection technologies,[11] signal processing, and proteomic biomarkers of infection. Developing this platform into a point-of-care device would overcome many of the problems associated with current state-of-the-art detection platforms used in ID diagnostics, such as high operating costs, low sensitivity, and limited multiplexing ability, while improving the speed of diagnosis. Major advances in preventing, treating, and monitoring IDs are therefore possible using this approach.

A few published reports on the integration of nano- with microtechnologies for biomolecular or viral detection have been described.[12–14] In these studies, the researchers used combinations of nanoparticles, microbeads, and microfluidics for detection. In all cases, reported detection sensitivities may be inadequate for clinical analysis. Furthermore, the experiments were not conducted in serum, which could affect the sensitivity because of interference from blood components.[15] Biobarcodes using gold nanoparticles have also been dem-

---

* Corresponding author. E-mail: warren.chan@utoronto.ca.
† Institute of Biomaterials and Biomedical Engineering and The Terrence Donnelly Centre for Cellular and Molecular Research, University of Toronto.
‡ Institute of Medical Sciences and the McLaughlin Centre for Molecular Medicine, University of Toronto.
§ Department of Materials Science, University of Toronto.
|| McLaughlin-Rotman Centre for Global Health, Tropical Disease Unit, UHN–Toronto General Hospital.
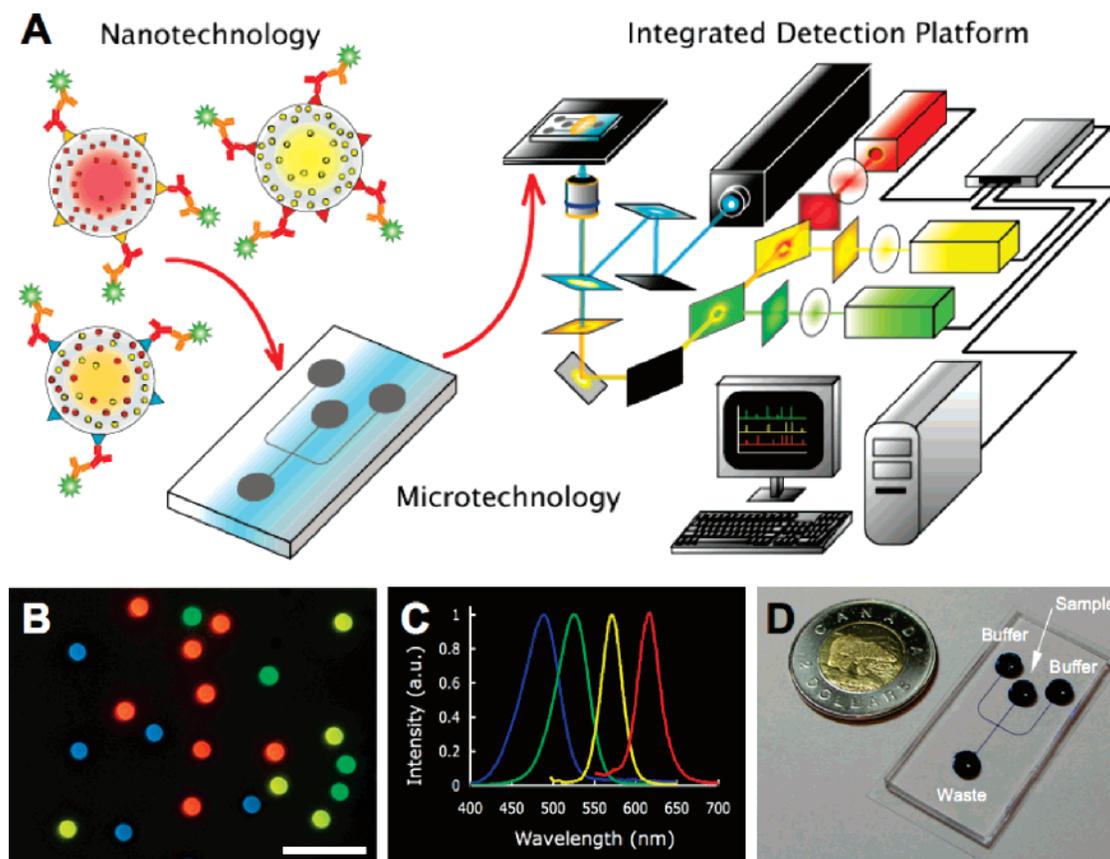
Figure 1. Diagnostic scheme. (A) Diagram illustrating the integration of QdotBs, solution-based sandwich assay, microfluidics and fluorescence detection with custom software for high throughput, multiplexed blood-borne pathogen detection (see Supporting Information for details). (B) Fluorescence image of a collection of different color emitting, 5.0 μm diameter polystyrene QdotBs suitable for proteomic or genomic assays (Olympus 40× objective, 0.75 NA, scale bar = 20 μm). (C) Normalized Qdot emission profiles corresponding to the Qdots used for the barcodes in (B), all excited using 365 nm light. (D) Sample microfluidic chip, fabricated in polydimethylsiloxane with wells labeled. Channel dimensions are 100 μm wide by 15 μm high. Blue dye was used to visualize the channel intersection for electrokinetic focusing.

onstrated for applications in molecular diagnostics.[16−18] The detection strategy requires multiple steps and amplification (e.g., silver staining) to achieve good assay detection sensitivity. Similarly, particles displaying unique graphic patterns for multiplexing purposes suffer from stringent, anisotropic orientation limitations during readout to enable detection.[19] In this paper, we present a detection system that only requires a few steps (after preparation of QdotBs), no amplification, and is simpler to use. Furthermore, unlike previous studies, we compare our results to FDA-approved methods and thus assess platform performance against current standards.

We selected three diagnostic targets (hepatitis B virus, HBV; hepatitis C virus, HCV, and human immunodeficiency virus, HIV) to demonstrate the utility of this integrated device for ID diagnostics. These three pathogens are all blood-borne viruses that use similar routes of transmission and are among the most prevalent IDs in the world. They are also leading causes of global morbidity and mortality. For example, HIV infects 40 million, HBV infects 400 million, and HCV infects 170 million people worldwide.[20−22] The majority of these cases of infection are located in the developing world. Current diagnostic schemes for detecting these infections require at least three separate tests, multiple return visits to

the clinic, and repeated blood samples before any present pathogens are detected. From an economic as well as an efficient diagnostic perspective, the implementation of a universal, multiplexed diagnostic tool with high sensitivity, specificity, and fast turnaround times has the potential to rapidly identify infected persons, initiate therapy, and subsequently curtail the transmission of highly infectious pathogens both in the developing and developed world.

There are four major components to this detection system (Figure 1A): (1) QdotBs conjugated to targeting molecules provide selectivity and multiplexing capabilities. The unique fluorescence signature from the barcode identifies the targeting molecule. (2) Electrokinetically driven microfluidics enables sequential, high-throughput readout of single barcodes with no movable parts and portability potential.[23] (3) Photon counting detection systems enable real-time readout of flowing barcodes. (4) Signal processing enables deconvolution of QdotB optical signals.

In this proof-of-concept experiment, we used the Nie method[6] to prepare three different QdotBs (QdotB1 contained 570 nm emitting ZnS-capped CdSe Qdots; QdotB2 contained 615 nm emitting Qdots; QdotB3 contained both 570 and 615 nm emitting Qdots; see Figure 2) for this study. It has been speculated that as many as 10^6 unique barcodes can be
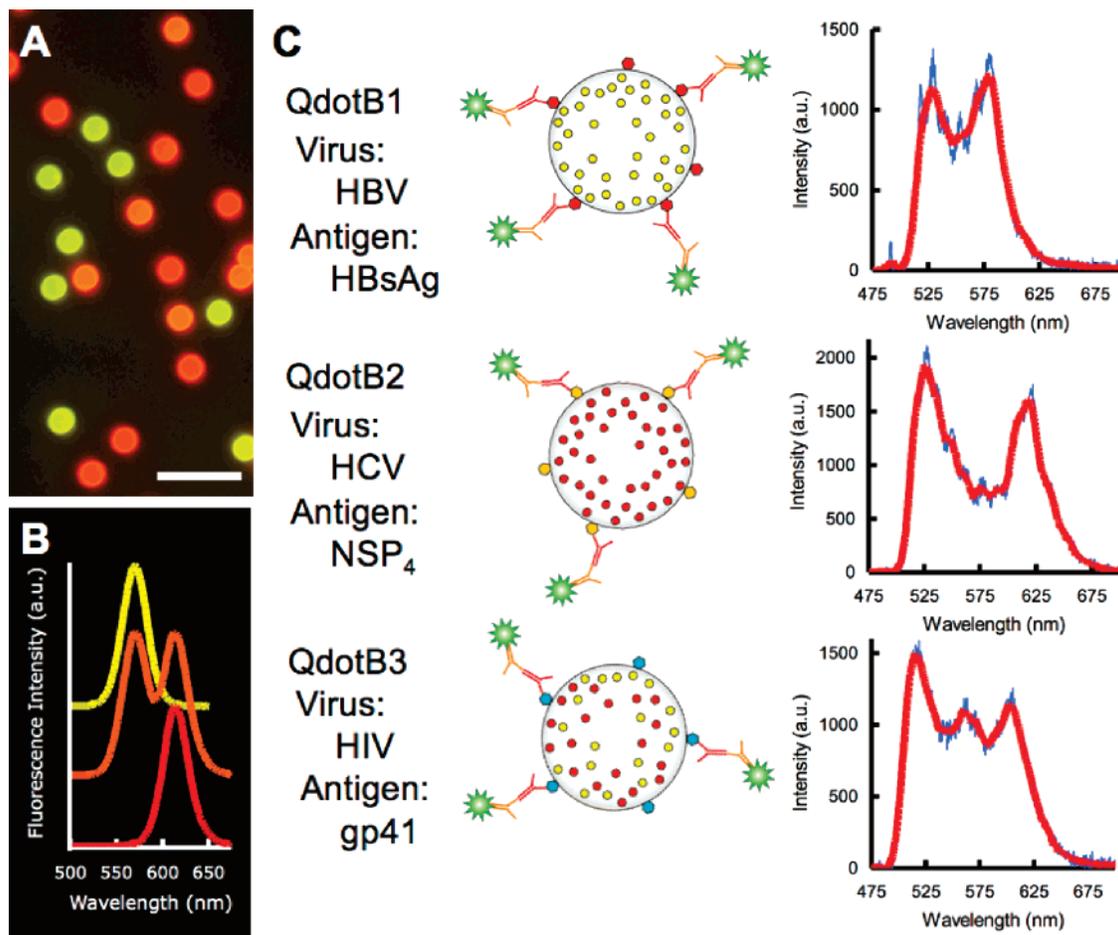
Figure 2. Sample QdotBs used for proof-of-concept experiments. (A) Fluorescence image of a collection of the three types of QdotBs used and (B) their corresponding Qdot profiles, offset for clarity (image taken using 40× objective, 0.75 NA, scale bar = 15 μm). (C) List of the different QdotBs with their corresponding surface conjugated antigens and fluorescence spectra. The peak around 520 nm is from AlexaFluor-488 dye molecules conjugated to the detection antibodies and indicates target molecule detection. Spectra were taken of assayed Qdot barcodes flowing in a microfluidic channel using 488 nm laser excitation (25 mW), with fluorescence collected using a 60× oil immersion objective (1.35 NA), a grating, and CCD camera (50 ms exposure time).

prepared using this approach because of the narrow spectral line widths and tunable fluorescence emissions of Qdots. If 10^6 barcodes are created, 10^6 biomarkers could in theory be identified simultaneously. Pathogen biomarkers (i.e., antigens) were covalently bound to the QdotB surface using carbodiimide chemistry.[24] The pathogen biomarkers were hepatitis B surface antigen (HBsAg), HCV nonstructural protein 4 (NSP$_4$), and HIV glycoprotein 41 (gp41). The QdotBs were then incubated in human serum spiked with corresponding antibodies for the conjugated viral antigens. Sandwich assay complexes (Figure 2C) were formed during a subsequent incubation with fluorophore−antibody conjugates (AlexaFluor-488 organic dye conjugated to goat anti-mouse IgG) to provide a fluorescence detection signal peak ~520 nm. Once antigen-coated QdotBs are prepared, the entire detection process, from biorecognition to measurement, takes less than 1 h (for detailed procedures, see Supporting Information Section S1).

QdotBs were loaded into the sample well of a disposable polydimethylsiloxane (PDMS) microfluidic chip (Figure 1D). These microfluidic chips were fabricated using conventional soft lithography techniques.[25,26] To induce hydrophilicity, the walls of the chips were treated with oxygen plasma. Electrokinetics, where electric fields propel fluids through small conduits, was used to transport QdotBs in the microchannels.[27] To minimize nonspecific binding of the QdotBs to the microchannel walls[28] and the associated aberrations in optical measurements, microfluidic flow focusing[29] was employed upstream of the detection window via a high voltage power supply and regulatory circuitry (see Supporting Information Section S2, Figure S1). As a QdotB passed through a focused laser spot (488 nm, 25 mW), the fluorescence signal was collected by a 60× oil immersion objective (1.35 NA). The signal passed through an optical train of dichroic mirrors, bandpass filters, and focusing lenses before illuminating solid-state photodetectors. These detectors have response times several orders of magnitude less than the time scale of a flowing bead, allowing for discrimination of single versus aggregated beads in the flow.[30] In a typical experiment, QdotBs are read at a rate of 70 barcodes per minute (see Supporting Information Section S3 for video S1 of QdotBs flowing in a microfluidic chip).

Once fluorescence emission reached the detectors, we observed large fluctuations in detector output voltages, which
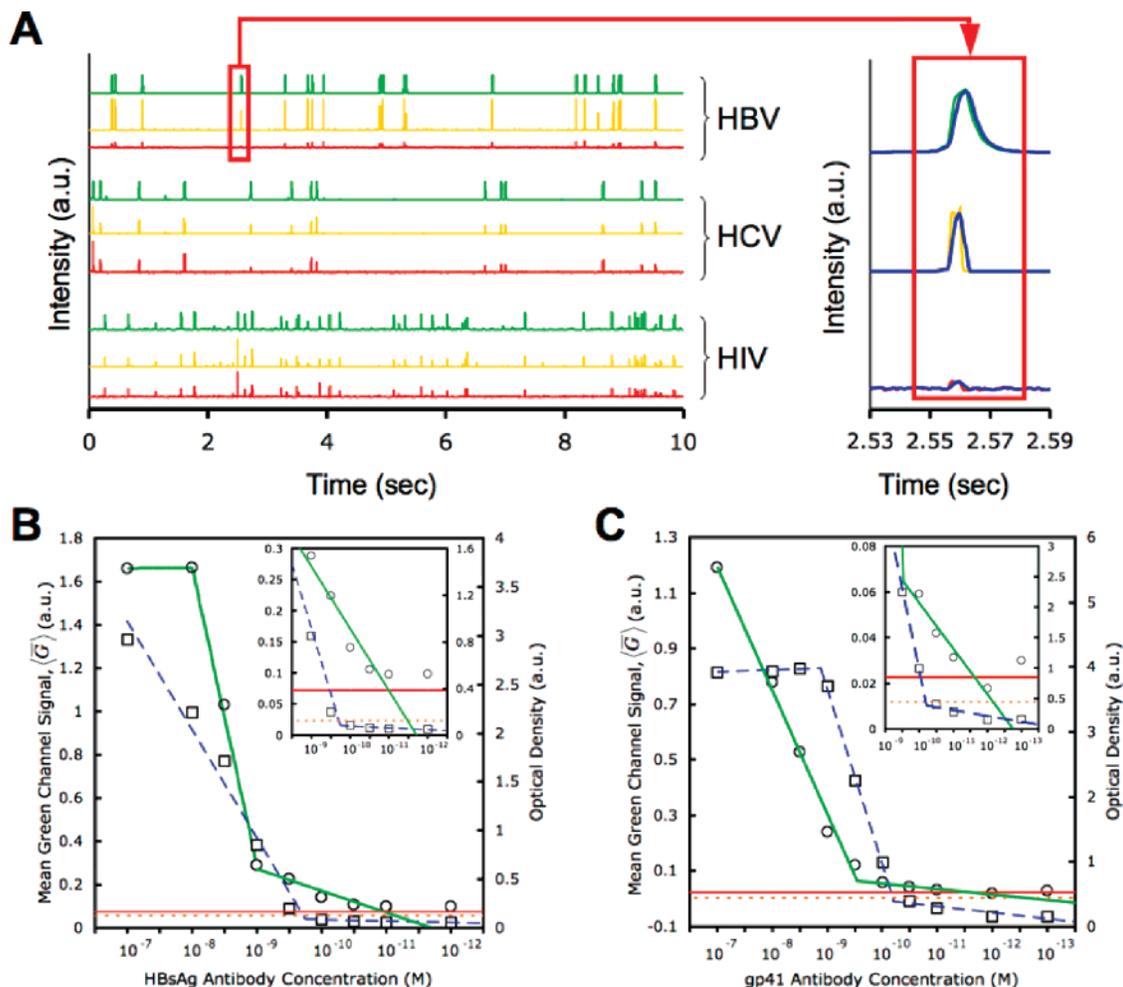
Figure 3. Detection sensitivity assessment. (A) Examples of photodetector data collected over 10 s intervals for HBV, HCV, and HIV detection sensitivity experiments. Each detector investigated a separate bandwidth determined by emission filters. The peaks from one HBV detection event are enlarged on the right, showing how detection peaks appear in all three channels. The slight variation in the width and tail of the top (green channel) peak compared with the peaks for the bottom two (yellow and red channels) illustrates different types of solid-state detectors being used within the detection platform. The bottom half of the figure shows detection sensitivity curves for (B) HBV and (C) HIV target antibodies using the detection system (solid green lines, ○) and FDA-approved ELISA kits (dashed blue lines, □). Each data point represents an average from three experiments (three microfluidic chips, each with separate samples). The red horizontal red lines set the system's detection limits. These lines correspond to the means plus 3 confidence intervals (95%) for control experiments (without target antibodies). ELISA was done in triplicates; the dashed horizontal lines represent the cutoff for detection sensitivities as specified by the kits' instructions. The insets show that, for both assays, the detection platform was 50-fold more sensitive than the commercial ELISA kits.

are indicators of detection. Figure 3A shows 10 s intervals of data collected during experiments. For these proof-of-concept studies, a PIN photodiode coupled to an optical power meter was used to examine green (500−540 nm) wavelengths, while avalanche photodiodes (APDs) were used for yellow and red bandwidths (560−590 and 600−660 nm, respectively). Outputs from all three detectors were relayed to a computer using a data acquisition card. Software developed in-house analyzed the collected data. Because the speed at which a QdotB traverses the laser spot is inversely proportional to the peak intensity measured by a detector (assuming no saturation), we normalized voltage peak values with respect to time. For example, the green channel, which indicates target antibody detection, used the metric $\langle G \rangle = (\int^{\text{peak}} V(t) \, dt)/(\int^{\text{peak}} dt)$, where $V(t)$ is the voltage signal as a function of time, t, and the average background noise is set

to zero. The yellow and red channels used metrics $\langle Y \rangle$ and $\langle R \rangle$, defined similarly.

Results obtained from serial dilutions of HBsAg and gp41 target antibodies are shown in Figure 3. For both anti-HBsAg and anti-gp41, the sensitivity limits were in the picomolar ($10^{-10}-10^{-12}$ M) range. When compared to FDA-approved kits with the same antigen and target antibody, we observed a 50-fold improvement in detection sensitivity. NSP$_4$ antibody sensitivity was also found to be in the picomolar range (see Supporting Information Section S2, Figure S2), however, no comparable FDA-approved ELISA kit exists. Limits of sensitivity were assessed by using three confidence intervals (95%) above the means for control (no antibody) samples because mean $\langle G \rangle$ values, $\overline{\langle G \rangle}$, are averaged from over 1000 QdotBs (see Supporting Information Section S4, tables S1 and S2, for data and statistical analysis).

A

Occurrence (Counts)

$\langle R\rangle/\langle Y\rangle$ Signal Ratio

B

Sample	Ag			Ab			AlexaFluor-488 anti-IgG	Notes
	HBV	HIV	HCV	HBV	HIV	HCV		
2 Pathogen Multiplex								
HBV+,HIV+	+	+	N/A	+	+	N/A	+	2 Ab
HBV+,HIV-	+	+	N/A	+	-	N/A	+	1 Ab
HBV-,HIV+	+	+	N/A	-	+	N/A	+	1 Ab
HBV-,HIV-	+	+	N/A	-	-	N/A	+	No Ab
Control 1	+	-	N/A	-	+	N/A	+	Cross-reactivity
Control 2	-	+	N/A	+	-	N/A	+	Cross-reactivity
Control 3	-	-	N/A	+	+	N/A	+	No Ag
Control 4	+	+	N/A	+	+	N/A	-	No Dye
3 Pathogen Multiplex								
HBV+,HIV+,HCV+	+	+	+	+	+	+	+	3 Ab
HBV-,HIV+,HCV+	+	+	+	-	+	+	+	2 Ab
HBV+,HIV+,HCV-	+	+	+	+	+	-	+	2 Ab
HBV+,HIV-,HCV+	+	+	+	+	-	+	+	2 Ab
HBV-,HIV-,HCV-	+	+	+	-	-	-	+	No Ab
Control 1	+	-	-	-	+	+	+	Cross-reactivity
Control 2	-	-	+	+	+	-	+	Cross-reactivity
Control 3	-	+	-	+	-	+	+	Cross-reactivity
Control 4	-	-	-	+	+	+	+	No Ag
Control 5	+	+	+	+	+	+	-	No Dye

C

Mean Green Channel Signal, $\langle G\rangle$ (a.u.)

Legend: HBV, HIV

HBV+,HIV+ — HBV+,HIV- — HBV-,HIV+ — HBV-,HIV- — Control 1 — Control 2 — Control 3 — Control 4

D

Mean Green Channel Signal, $\langle G\rangle$ (a.u.)

Legend: HBV, HIV, HCV

HBV+,HIV+,HCV+ — HBV-,HIV+,HCV+ — HBV+,HIV+,HCV- — HBV+,HIV-,HCV+ — HBV-,HIV-,HCV- — Control 1 — Control 2 — Control 3 — Control 4 — Control 5
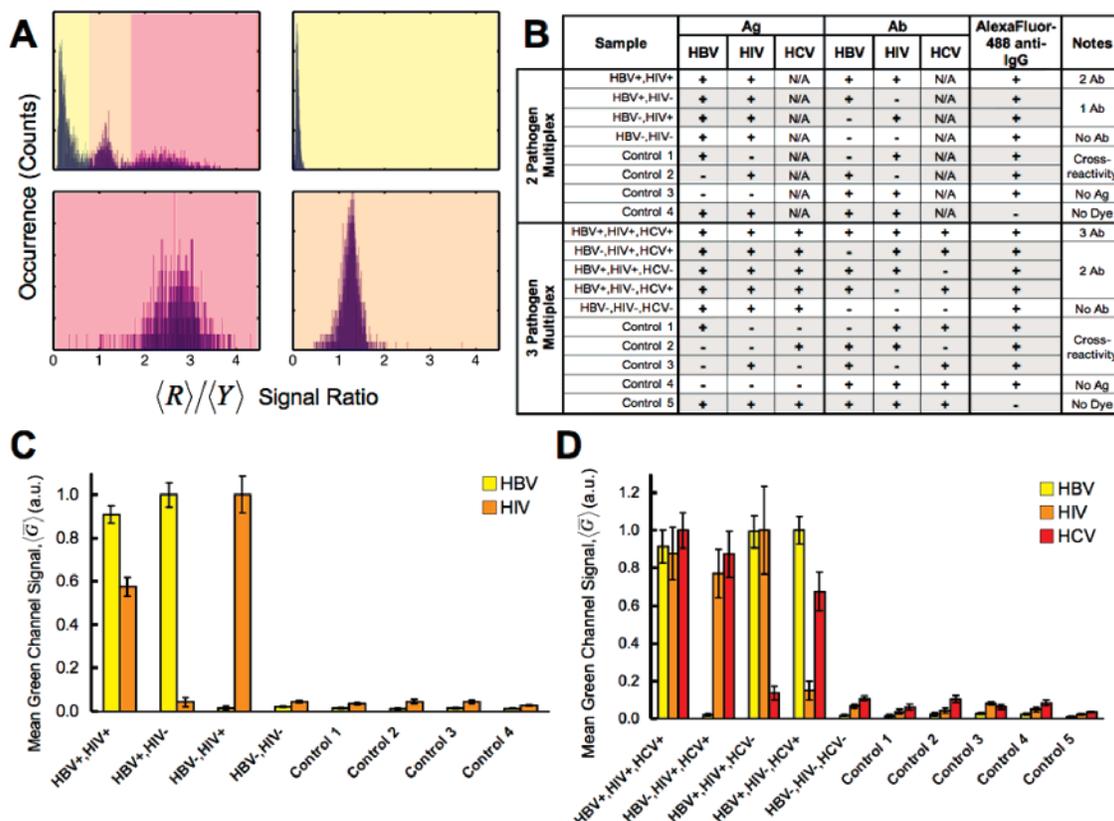
Figure 4. Multiplexed infectious disease detection. (A) Histograms of $\langle R\rangle/\langle Y\rangle$ signal ratios for (clockwise starting at the top right) HBV only, HIV only, HCV only, and all three pathogens multiplexed in assays. The signal ratios are used to identify the barcodes and hence the viral markers. (B) Table of experiments used for (C) and (D). (C) Results of two-pathogen multiplexing experiments with HBV and HIV. (D) Results of three-pathogen multiplexing experiments with HBV, HCV, and HIV. These results show negligible cross-reactivity for these three pathogen markers. Concentrations of HBV, HIV, and HCV antibodies for this study were all 4.74×10^{-9} M. Error bars represent one standard deviation.

The system also demonstrated multiplexed detection of the pathogens. Figure 4 shows results of two (HBV and HIV) and three (HBV, HCV, and HIV) pathogen multiplexing and control experiments. The use of multiple QdotBs necessitated a barcode discrimination strategy. The detector data was analyzed by first indicating the presence of yellow channel peaks and then classified as HBV, HCV, or HIV detection events based on the value of the $\langle R\rangle/\langle Y\rangle$ ratio. Figure 4A shows histograms of detection events from HBV, HIV, and HCV and that there are distinguishable differences in the $\langle R\rangle/\langle Y\rangle$ ratios, from low to medium to high, respectively (see Supporting Information Section S4, Tables S3 and S4 for data and statistical analysis). By using this simple approach, it was possible to classify detection events according to QdotB signal and hence, the targeting molecule for the pathogen of interest. As the number of QdotBs used in multiplexed assays increases, this method of using signal ratio distributions should become increasingly important.

The use of QdotB probes for multiplexed fluorescence detection has many advantages for medical diagnostics, including the narrow and tunable profiles of Qdots that allow for numerous QdotBs to be synthesized and integrated into large-scale multiplexed assays.[31−33] Also, the detection technique is simple and easy to conceptualize, important for training system operators in developing regions of the world.

But perhaps most importantly, QdotBs allow for the detection signal and barcode identification to be of the same format (fluorescence), shortening analysis algorithms, and decreasing the number of steps necessary for detection. For example, graphically unique barcodes that incorporate fluorescence for detection of analytes require a fluorescence algorithm and an algorithm to identify the graphic pattern.[19] Similarly, the biobarcode system, which uses oligonucleotide sequences for barcoding, requires sequestering (and possible amplification steps) of the oligo identifier strands.[18] By exploiting the tunability of fluorescence emission profiles using collections of Qdots, biomolecular detection and barcode identification signals are integrated, greatly simplifying the detection scheme. Furthermore, with the advance of near-infrared (NIR) emitting Qdots,[34−36] the number of different populations of Qdots that can be incorporated into these QdotBs is large, greatly expanding potential size of a combinatoric QdotB library.

Fluorescence is a popular detection method because it is typically visible to the naked eye and its signal is more sensitive than most other spectroscopy-based analytical detection methods such as absorbance. Although we demonstrated only 50 times greater sensitivity than current FDA-approved diagnostic methods, the sensitivity could be further enhanced in the future. In these experiments, we used organic dyes and polarized laser light in the current detection system,

where the anisotropy of the dye molecule dipole moment on the surface of the QdotBs results in less efficient excitation of detection fluorophores and hence a lower detection signal. By conjugating individual, water solubilized Qdots to the detection antibodies, which possess isotropic dipole moments and larger absorption cross sections than organic dyes, the detection signal should be significantly increased. Inspite of this shortcoming, the detection results were still better than for ELISA kits, which is likely due to enhanced assay capture efficiency of microbeads over flat surfaces.[37,38]

To optimize multiplexed detection, care must be taken to avoid or minimize the effects of assay interferences. These interferences can range from nonspecific interactions to using target-detection molecular systems with similar capture affinities. One would expect that, as the number of targets increases, regardless of the detection platform type, these interferences could be problematic. By targeting structurally unique epitopes of each pathogen biomarker, accurate and reproducible multiplexed proteomic assays should be quite feasible. Furthermore, as the number of multiplexed targets increases, an increase in the complexity of any associated algorithm also increases. For this platform, optical signals are collected using a set of spectral bands. For a collection of n fluorophores and n spectral bands, it is always possible to determine the relative contributions (intensities) of a given fluorophore to the overall signal as long as each fluorophore signal distributes across the n spectral bands (or crosstalks) uniquely. In theory, fluorophores should crosstalk uniquely if their spectral profiles are sufficiently different, which is generally correct for populations of different color Qdots. Hence, when expanding the QdotB library, the algorithm will become increasingly more complex but good characterization of QdotB spectral crosstalk behavior before use should make this issue manageable.

We demonstrated the successful convergence of nano- and microtechnologies with molecular diagnostics for high-throughput, multiplexed detection of ID protein biomarkers. To advance this technology, future developments should include the synthesis of large sets of QdotBs and corresponding algorithms to deconvolve optical signals of increasing complexity. This would allow for the simultaneous analysis of larger numbers of biomarkers. The assay protocols could also be integrated into the microfluidic chip to minimize human involvement in the entire detection scheme. With the use of Qdots for preparing the barcodes and rapid advances in optical technology, this format could be miniaturized into a handheld device for portability. Such a platform could use a photonic chip with integrated solid-state detectors for optical detection, while the microfluidic chip remains separate and disposable. Finally, with QdotB targets already prepared, the entire assay is cost-effective (see Supporting Information Section S5) and readout requires less than 1 h, making it useful for rapidly screening samples for a large number of globally important infectious diseases. This platform could also be adapted toward screening for biomarkers of other diseases such as cancer or heart disease. In conclusion, this approach shows promise for large-scale, high-throughput multiplexed biomolecular detection of many serious blood-borne illnesses and should lead to the development of a handheld point-of-care diagnostic.

Supporting Information Available: Available in Section S1 are details of the experimental protocols for Qdot and QdotB synthesis, microfabrication, QdotB assays, performed ELISAs, detection experiments, collection of QdotB spectra, QdotB imaging, and the QdotB detection algorithm. Figures illustrating the voltage regulation circuit for electrokinetic flow and a dilution sensitivity curve for anti-HCV NSP$_4$ antibodies are found in Section S2. A short movie (AVI) is provided of different QdotBs flowing in different regions of the microfluidic channel with captions describing each segment given in Section S3. Tables of the experimental results collected for the sensitivity and multiplexing experiments are provided in Section S4, followed by a cost analysis for a single assay in Section S5. This material is available free of charge via the Internet at http://pubs.acs.org.

References

(1) Burda, C.; Chen, X.; Narayanan, R.; El-Sayed, M. A. *Chem. Rev.* **2005**, *105*, 1025.
(2) Squires, T. M.; Quake, S. R. *Rev. Mod. Phys.* **2005**, *77*, 977.
(3) Alivisatos, A. P. *J. Phys. Chem.* **1996**, *100*, 13226.
(4) Shatz, G. *Proc. Natl. Acad. Sci. U.S.A.* **2007**, *104*, 6885.
(5) Yager, P.; Edwards, T.; Fu, E.; Helton, K.; Nelson, K.; Tam, M. R.; Weigl, B. H. *Nature* **2006**, *442*, 412.
(6) Han, M.; Gao, X.; Su, J. Z.; Nie, S. *Nat. Biotechnol.* **2001**, *19*, 631.
(7) Klostranec, J. M.; Chan, W. C. W. *Adv. Mater.* **2006**, *18*, 1953.
(8) Burns, M. A.; Johnson, B. N.; Brahmasandra, S. N.; Handique, K.; Webster, J. R.; Krishnan, M.; Sammarco, T. S.; Man, P. M.; Jones, D.; Heldsinger, D.; Mastrangelo, C. H.; Burke, D. T. *Science* **1998**, *282*, 484.
(9) Kopp, M. U.; de Mello, A. J.; Manz, A. *Science* **1998**, *280*, 1046.
(10) Huang, B.; Wu, H.; Bhaya, D.; Grossman, A.; Granier, S.; Kobilka, B. K.; Zare, R. N. *Science* **2007**, *315*, 81.
(11) Yotter, R. A.; Wilson, D. M. *IEEE Sens. J.* **2003**, *3*, 288.
(12) Liu, W.; Zhu, L.; Qin, Q.; Zhang, Q.; Feng, H.; Ang, S. *Lab Chip* **2005**, *5*, 1327.
(13) Yun, K.; Lee, D.; Kim, H.; Yoon, E. *Meas. Sci. Technol.* **2006**, *17*, 3178.
(14) Steigert, J.; Grumann, M.; Brenner, T.; Mittenbuhler, K.; Nann, T.; Ruhe, J.; Moser, I.; Haberle, S.; Riegger, L.; Riegler, J.; Bessler, W.; Zengerie, R.; Ducree, J. *J. Assoc. Lab. Autom.* **2005**, *10*, 331.
(15) Tate, J.; Ward, G. *Clin. Biochem. Rev.* **2004**, *25*, 105.
(16) Stoeva, S. I.; Lee, J.; Thaxton, C. S.; Mirkin, C. A. *Angew. Chem., Int. Ed.* **2006**, *45*, 3303.
(17) Stoeva, S. I.; Lee, J.; Smith, J. E.; Rosen, S. T.; Mirkin, C. A. *J. Am. Chem. Soc.* **2006**, *128*, 8378.
(18) Goluch, E. D.; Nam, J.; Georganopoulou, D. G.; Chiesl, T. N.; Shaikh, K. A.; Ryu, K. S.; Barron, A. E.; Mirkin, C. A.; Liu, C. *Lab Chip* **2006**, *6*, 1293.
(19) Pregibon, D. C.; Toner, M.; Doyle, P. *Science* **2007**, *315*, 1393.
(20) Fauci, A. S.; Mavilio, D.; Kottilil, S. *Nat. Rev. Immunol.* **2005**, *5*, 835.

(21) Lai, C.; Ratziu, V.; Yuen, M.; Poynard, M. *Lancet* **2003**, *362*, 2089.

(22) Poynard, T.; Yuen, M.; Ratziu, V.; Lai, C. *Lancet* **2003**, *362*, 2095.

(23) Erickson, D.; Sinton, D.; Li, D. *Lab Chip* **2004**, *4*, 87.

(24) Rogers, P. H.; Michel, E.; Bauer, C. A.; Vanderet, S.; Hansen, D.; Roberts, B. K.; Calvez, A.; Crews, J. B.; Lau, K. O.; Wood, A.; Pine, D. J.; Schwartz, P. V. *Langmuir* **2005**, *21*, 5562.

(25) Xia, Y.; Whitesides, G. M. *Annu. Rev. Mater. Sci.* **1998**, *28*, 153.

(26) Unger, M. A.; Chou, H.; Thorsen, T.; Scherer, A.; Quake, S. R. *Science* **2000**, *288*, 113.

(27) Ghosal, S. *Annu. Rev. Fluid Mech.* **2006**, *38*, 309.

(28) Toepke, M. W.; Beebe, D. J. *Lab Chip* **2006**, *6*, 1484.

(29) Xuan, X.; Li, D. *Electrophoresis* **2005**, *26*, 3552.

(30) In a similar step-up, we used a spectrograph and CCD camera to collect spectra from flowing beads. However, the camera's 50 ms integration time was too long to ensure spectra corresponded to individual QdotBs when flowing at speeds on the order of 1 mm/s.

(31) Ghazani, A. A.; Lee, J. A.; Klostranec, J.; Xiang, Q.; Dacosta, R. S.; Wilson, B. C.; Tsao, M. S.; Chan, W. C. W. *Nano Lett.* **2006**, *6*, 2881.

(32) Xing, Y.; Chandry, Q.; Shen, C.; Kong, K. Y.; Zhau, H. E.; Chung, L. W.; Petros, J. A.; O'Reagan, R. M.; Yezhelyev, M. V.; Simons, J. W.; Wang, M. D.; Nie, S. *Nat. Protocols* **2007**, *2*, 1152.

(33) Jiang, W.; Papa, E.; Fischer, H.; Mardyani, S.; Chan, W. C. W. *Trends Biotechnol.* **2004**, *22*, 607.

(34) Weissleder, R. *Nat. Biotechnol.* **2001**, *19*, 316.

(35) Jiang, W.; Singhal, A.; Zheng, J.; Wang, C.; Chan, W. C. W. *Chem. Mater.* **2006**, *18*, 4845.

(36) Bailey, R. E.; Nie, S. *J. Am. Chem. Soc.* **2003**, *125*, 7100.

(37) Stenberg, M.; Stiblert, L.; Nygren, H. *J. Theor. Biol.* **1986**, *120*, 129.

(38) Stenberg, M.; Nygren, H. *J. Immunol. Methods* **1988**, *113*, 3.